NORTHWESTERN UNIVERSITY

McCORMICK SCHOOL OF ENGINEERING AND APPLIED SCIENCE

DEPARTMENT OF MATERIALS SCIENCE

TECHNICAL REPORT # 28

NOVEMBER 1990

OFFICE OF NAVAL RESEARCH

CONTRACT NO. N00014-80-C-116

LOAD SHARING OF THE PHASES IN 1080 STEEL DURING LOW CYCLE FATIGUE

BY

R. A. WINHOLTZ AND J. B. COHEN

EVANSTON, ILLINOIS

Load Sharing of the Phases in 1080 Steel During Low Cycle Fatigue

R. A. Winholtz and J.B. Cohen

Department of Materials Science and Engineering, The Robert R. McCormick School of Engineering and Applied Science, Northwestern University, Evanston, IL 60208

Abstract

By means of x-ray diffraction, the stress response of the individual phases in a 1080 steel were measured. Specimens with pearlitic, spheroidal, and tempered martensitic microstructures were subjected to low cycle fatigue and the stress strain hysteresis loops were separated into components for the carbide and matrix phases. These results show that as the material yields in both tension and compression the carbides take a higher fraction of the load and thus the stress range experienced by the carbide phase is much higher than the matrix during low cycle fatigue.

I. Introduction

Most engineering materials are inhomogeneous and the macroscopic mechanical behavior will be a composite of the behaviors of the material's components and their interactions. These components can be different phases, composition fluctuations, or even grains with different orientations. While the overall composite behavior is useful for many purposes a more complete understanding of the material properties requires a knowledge of the behaviors and interactions of the different components of the material.

Stress measurements with diffraction provide a unique probe to study the mechanical behavior of the individual phases in a multiphase material. Different diffraction peaks arise from the different phases and only sample that volume in the material containing the phase from which a peak arises. The diffraction peaks thus provide information on the individual phases in multiphase or composite materials. In this study we have, for the first time, used the diffraction peak shifts in a plain carbon steel to measure the individual stress responses of the matrix and carbide phases in a 1080 steel subjected to cyclic plastic strain.

Residual stresses are known to play a significant role in fatigue failure. Changes in residual stresses have been measured often in steel but usually only in the ferrite phase. The role of stresses in the carbide phase has been largely ignored. Since steel and many other materials are multiphase it is therefore important to know the residual stress state of all the phases and their relation to the fatigue process.

Steel was chosen for this study because of its historical and technological importance. The mechanical properties of steel are strongly affected by of the amount and morphology of the carbides present which may be controlled by heat treatment. It is of interest to know how the individual phases interact to produce the bulk mechanical response of the material. With a proper understanding of the macro- and micro-stresses present in a material (from x-ray diffraction stress measurements) we may separate the stress response of the phases and study the effects of carbide morphology on the low cycle fatigue properties of a steel.

Wilson and Konnan [1] and Hanabusa, Fukura and Fujiwara [2] have studied the interaction stresses between the ferrite and cementite phases of steel during tensile deformation and reported that large tensile interaction stresses develop in the cementite. In both of these works the stresses in the cementite were measured with a

very low angle diffraction peak (~55° 2θ) which gives large instrumental errors in the measurements. Quesnel, Meshii and Cohen have measured the residual stresses in only the ferrite phase of a high strength low alloy steel after low cycle fatigue.[3,4] The data indicated an inhomogeneous distribution of stress which changed depending on whether the test was finished releasing from tension or from compression. The total-stress also reversed sign with each load reversal. The present work was intended to clarify the residual stresses present and the roles of the matrix and carbide phases in the low cycle fatigue of steel.

II. Theory

A. *Macro- and Micro-stresses*

In a multiphase material both macro- and micro-stresses will exist.[5,6,7] The macro-stress is the component of stress that is by definition the same in every phase in a material. Residual macro-stresses arise from the differential deformation of one region of a material relative to another. These are the stresses that would be measured by dissection methods and therefore are assumed to vary on a scale large compared to the microstructure. The stresses in an inhomogeneous material will differ point to point from those predicted for a homogeneous material and it is these differences that are termed micro-stresses. These will arise from a variety of causes, such as different plastic behavior of the phases, or differential thermal expansion. Micro-stresses vary on the scale of the microstucture and must balance to zero between the phases.

Considering a two phase material, the total stress in a phase is the sum of the macro-stress and the micro-stress,

$$\langle {}^{t\,\alpha}\sigma_{ij} \rangle = {}^{M}\sigma_{ij} + \langle {}^{\mu\,\alpha}\sigma_{ij} \rangle \qquad (1)$$

$$\langle {}^{t\,\beta}\sigma_{ij} \rangle = {}^{M}\sigma_{ij} + \langle {}^{\mu\,\beta}\sigma_{ij} \rangle \; . \qquad (2)$$

In these equations the superscripts t, M, and μ represent the total-stress, the macro-stress, and the micro-stress respectively and the superscripts α and β designate the phase. Since we will be dealing with x-ray measurements, which measure an average over the sampling volume, carets are used to indicate averages. Equations 1

and 2 are valid for each of the six components of the stress tensors. Equilibrium relations for micro-stresses require that the average micro-stresses weighted by their volume fraction must sum to zero.[5] For a two phase material we have

$$(1-f)\langle {}^{\mu}\sigma^{\alpha}_{ij}\rangle + f\langle {}^{\mu}\sigma^{\beta}_{ij}\rangle = 0 \ . \tag{3}$$

Here f is the volume fraction of the β phase and (1-f) is the volume fraction of the α phase. By measuring the total stress tensors in each phase we may determine the macro-stress tensor and the micro-stress tensors in each phase from Equations 1, 2, and 3. All the stresses ${}^{M}\sigma_{i3}$ and ${}^{\mu}\sigma_{i3}$ must be zero at the surface. If gradients of the macro-stresses in the surface are zero, equilibrium relations require that the macro-stress components perpendicular to to the surface must be zero at all depths of the material

$${}^{M}\sigma_{i3} = 0 \ . \tag{4}$$

This is not true for the micro-stresses however.[5]

B. *Stress Measurement with Diffraction*

Stresses may be measured via diffraction by using the crystal lattice as an internal strain gauge.[7] By measuring the interplanar spacing at a number of different tilts of the specimen, the strain tensor may be obtained. From the strain tensor the stress tensor may be determined from Hooke's law by using the appropriate x-ray elastic constants. In Figure 1 the laboratory (L_i) and sample (S_i) coordinate systems are shown. The sample coordinate system is the one in which the measured stresses will be referenced while the laboratory system is the one in which the diffraction measurements will be made. The two coordinate systems are rotated with respect to each other by the angles ϕ and ψ. By orienting the diffraction vector along the L_3 axis the interplanar spacing along that direction may be measured by determining the position of the diffraction peak using Bragg's law:

$$\lambda = 2\langle d^{\alpha}_{\phi\psi}\rangle \sin\theta_p \ . \tag{5}$$

In this equation λ is the x-ray wavelength, $\langle d^{\alpha}_{\phi\psi} \rangle$ is the average interplanar spacing in the α phase along the L_3 axis, and θ_p is one half of the scattering angle of the peak. Using the unstressed interplanar spacing d_0, we may write the strain along the L_3 axis in terms of the strains in the sample coordinate system.[8]

$$\langle \varepsilon^{\alpha}_{\phi\psi} \rangle = \frac{\langle d^{\alpha}_{\phi\psi} \rangle - d^{\alpha}_{0}}{d^{\alpha}_{0}} = \langle \varepsilon^{\alpha}_{11} \rangle \cos^2\phi \sin^2\psi + \langle \varepsilon^{\alpha}_{22} \rangle \sin^2\phi \sin^2\psi + \langle \varepsilon^{\alpha}_{33} \rangle \cos^2\psi + \langle \varepsilon^{\alpha}_{12} \rangle \sin 2\phi \sin^2\psi + \langle \varepsilon^{\alpha}_{13} \rangle \cos\phi \sin 2\psi + \langle \varepsilon^{\alpha}_{23} \rangle \sin\phi \sin 2\psi \qquad (6)$$

By measuring a number of peak positions at different ϕ and ψ values this equation may be solved for the strains in the sample coordinate system by a least-squares procedure.[9] The stress tensor may then be obtained using Hooke's law:

$$\sigma^{\alpha}_{ij} = \frac{1}{S^{\alpha}_2/2} \varepsilon^{\alpha}_{ij} - \delta_{ij} \frac{S^{\alpha}_1}{S^{\alpha}_2/2(S^{\alpha}_2/2 + 3S^{\alpha}_1)} \varepsilon^{\alpha}_{kk} . \qquad (7)$$

Here S_1 and $S_2/2$ are the diffraction elastic constants[7,10] and δ_{ij} is the Krönecker delta function. To solve Equation 6 for the strains and hence stresses an accurate value of the unstressed d-spacing is needed which may be difficult to obtain.[11] Errors in the unstressed lattice parameter lead to an error in the hydrostatic component of the stress and strain tensors.[12]

The stress tensor may be separated into a hydrostatic component and a deviatoric component.:

$$\sigma_{ij} = \delta_{ij} \tau_H + \tau_{ij} , \qquad (8)$$

where the hydrostatic stress τ_H is:

$$\tau_H = (\sigma_{11} + \sigma_{22} + \sigma_{33})/3 . \qquad (9)$$

Substituting Equations 7, 8, and 9 into Equation 6 and solving for the measured d-spacing we have:[12]

$$\langle d^{\alpha}_{\phi\psi} \rangle = \langle {}^{t}\tau^{\alpha}_{H} \rangle d^{\alpha}_{0} [S^{\alpha}_{2}/2 + 3S^{\alpha}_{1}] - [\langle {}^{t}\tau^{\alpha}_{11} \rangle + \langle {}^{t}\tau^{\alpha}_{22} \rangle] d^{\alpha}_{0} S^{\alpha}_{2}/2 + d^{\alpha}_{0}$$
$$+ \langle {}^{t}\tau^{\alpha}_{11} \rangle d^{\alpha}_{0} S^{\alpha}_{2}/2 (1 + \cos^{2}\phi) \sin^{2}\psi$$
$$+ \langle {}^{t}\tau^{\alpha}_{22} \rangle d^{\alpha}_{0} S^{\alpha}_{2}/2 (1 + \sin^{2}\phi) \sin^{2}\psi$$
$$+ \langle {}^{t}\tau^{\alpha}_{12} \rangle d^{\alpha}_{0} S^{\alpha}_{2}/2 \sin 2\phi \sin^{2}\psi$$
$$+ \langle {}^{t}\tau^{\alpha}_{13} \rangle d^{\alpha}_{0} S^{\alpha}_{2}/2 \cos\phi \sin 2\psi$$
$$+ \langle {}^{t}\tau^{\alpha}_{23} \rangle d^{\alpha}_{0} S^{\alpha}_{2}/2 \sin\phi \sin 2\psi \quad . \qquad (10)$$

Here ${}^{t}\tau^{\alpha}_{H}$ is the hydrostatic component of the stress tensor and ${}^{t}\tau^{\alpha}_{ij}$ are the deviatoric components of the stress tensor present in the α-phase of the specimen. By measuring a collection of d-spacings and using the relation:

$$\langle {}^{t}\tau^{\alpha}_{11} \rangle + \langle {}^{t}\tau^{\alpha}_{22} \rangle + \langle {}^{t}\tau^{\alpha}_{33} \rangle = 0 , \qquad (11)$$

which holds for deviatoric tensors, Equation 10 may be solved for the deviatoric stresses without accurate values of d^{α}_{0} since it is only a multiplier in the deviatoric components. The hydrostatic component of stress is part of three constant terms in Equation 10 and cannot be determined without an accurate value of d^{α}_{0}.[12] Note also that only the elastic constant $S_2/2$ is needed to determine the deviatoric stresses. Equations 1, 2, and 3 also hold for deviatoric stress tensors. Thus the deviatoric macro- and micro-stress tensors may be obtained without accurate values of d_0 for the different phases in a multiphase material. The hydrostatic macro-stress may be determined because ${}^{M}\sigma_{33}$ must be zero. Thus, with Equation 8 the hydrostatic component of the macro-stress is:[12]

$$\overset{M}{\tau}_{H} = - \overset{M}{\tau}_{33} . \qquad (12)$$

Yield and plastic flow of materials are not sensitive to the hydrostatic stress and the deviatoric stress tensor is sufficient to investigate these material properties. In what follows all tensors presented will be deviatoric stress tensors.

Finally, it should be noted that with diffraction only the elastic component of the strain tensor is measured; any plastic strains are not determinable via diffraction. Strains measured with diffraction are also along a particular crystallographic direction that has its own elastic constants which will in general differ from the bulk values, and will vary with preferred orientation.

C. Deformation of Two Phase Materials

When a two phase material is subjected to uniaxial tensile strain along the P_1 axis it will behave similar to the schematic shown in Figure 2. The bulk material will have a stress response that is elastic to the yield point where it will deform plastically with a nonlinear stress response. The stress response of the bulk material is that measured by traditional mechanical testing methods (i.e. a load cell) and is by definition the macro-stress applied to the sample $\overset{Appl}{\tau}_{11}$. The material is heterogeneous however and each point in the material will have its own individual response to the applied strain. The bulk response is the average of the responses of all points in the material volume. For a two phase material the average stress in the individual phases will be different than the bulk stress giving rise to micro-stresses as shown in the figure. The average micro-stresses must obey Equation 3. (In this figure the elastic response of the two phases is assumed to be the same, which need not be the case.)

After deformation, if the bulk stress is removed, the bulk material will relax elastically retaining a plastic offset. The individual phases will not relax to zero but the micro-stresses will be retained as shown. These micro-stresses are retained without the external load applied and may be measured via diffraction. If the bulk stress at the release of the specimen is known, the individual stress response of the individual phases may be inferred by adding back the applied stress $\overset{Appl}{\tau}_{11}$ to micro-stresses measured after the load is released. Thus with a proper understanding of the macro- and micro-stresses the mechanical response of the individual phases may be determined even if the diffraction stress measurements cannot be made in situ on the

material as it is mechanically loaded (although this could, in principle, be done).

III. Experimental Methods

A. *Materials*

A near eutectoid 1080 plain carbon steel was chosen to maximize the diffracted intensity from the cementite phase without adding the complications of proeutectoid cementite. Also, with a plain carbon steel complications from alloy carbides are avoided.

Steel in the form of 0.794 cm (5/16 inch) hot rolled sheet was obtained from Amtex Steel Inc. (Chicago, IL). Fatigue specimens as shown in Figure 3 were machined from the center of the plate with the rolling direction corresponding to the loading axis as shown in Figure 3. After machining, the specimens were polished through 600 grit with SiC paper, the final scratches running along the loading direction of the specimens. Final polishing was done before heat treating so that any residual stresses from the polishing would be removed during heat treatment.

The samples were then heat treated to form three different microstructures: pearlite, spheroidite, and tempered martensite. To produce a pearlitic microstructure the specimens were austenitized for 15 minutes at 1073 K in an argon atmosphere to prevent decarburization and then allowed to cool outside the hot zone of the furnace. Spheroidized specimens were heated at 973 K for ten hours in a vacuum of 10^{-6} torr to prevent decarburization. Tempered martensite was produced by austenitizing specimens for 15 minutes at 1073 K in an argon atmosphere and quenching into water followed by tempering for four hours at 773 K in vacuum. The tempered martensite specimens were repolished between quenching and tempering to remove the scale that formed upon quenching and leave a surface suitable for the x-ray diffraction measurements. Samples were examined metallographically to be sure that decarburization of the surface had not occurred.

B. *Diffraction Measurements*

In making the stress measurements, determining the diffraction peak positions from the cementite phase was difficult. A high angle diffraction peak and sufficient diffracted intensity are needed for accuracy and precision in the stress measurement.

By using a chromium plated copper rotating anode target, chromium characteristic radiation was obtained with sufficient intensity to measure the stresses in the cementite phase.[12] The 211 peak at about 156° 2θ was used for the ferrite phase and the 250 peak at about 148° 2θ for the cementite phase. Figure 4 shows an example of the cementite peak. To improve the peak to background ratio for the cementite peaks a Li drifted Si solid state detector was used to eliminate fluorescence from the specimens originating from the white spectrum in the incident beam. The peak to background ratio was not as good as when using a diffracted beam monochromator, however, the greater intensity measured with the solid state detector was deemed to provide the best method for measuring the diffracted intensity.

Because the 250 cementite diffraction peak is located on the tail of the 211 ferrite peak, the background intensity will vary underneath the cementite peak depending on the breadth of the ferrite peak which varies with sample tilt. This will cause the position of maximum intensity in the diffraction pattern to differ from the peak position of diffracted intensity arising from the 250 cementite peak. Thus the peak positions were not determined by fitting the top portion to a parabola, which is traditionally done in stress measurement, but were determined by fitting the entire peak to a nonlinear function representing the peak and the background intensity.

The diffraction peak positions were determined by fitting pseudo-Voigt functions, including $K\alpha_1$ and $K\alpha_2$ doublets, to the diffraction peaks.[13] The matrix peak fits employed a linear background while with the cementite peaks an exponential plus linear background was included to account for the tail of the matrix peak. The nonlinear functional fits were done with a Levenberg-Marquardt algorithm which also provides an estimate of the error in the peak location based on the counting statistics of the diffraction scans.[14] These errors may then be propagated through to the strain and stress tensors.[7,9]

The tempered martensite microstructure proved the most difficult one in which to observe the cementite peaks. The matrix peaks are broadened because the martensitic transformation highly strains the lattice. (In specimens tempered at a lower temperature or for less time the cementite peak could not be accurately fit at all with the given diffraction equipment.) The errors in the measurements on the tempered martensite are therefore significantly higher than those for pearlite or spheroidite.

The instrument was optimized for intensity and not resolution. The horizontal

beam divergence was 1.5° while the vertical divergence was 1.4°. The goniometer radius was 216 mm, the beam size on the specimen was about 5 by 5 mm, and the receiving slit was 1.25 mm. The target was aligned in point focus to optimize intensity for a beam slitted down to fit on a fatigue specimen. The specimen surface was positioned to within 0.004 mm (0.001 inch) of the center of the diffractometer by determining the lattice parameter for each of the different ferrite peaks and repositioning the specimen with a dial indicator.[7]

The matrix peaks were scanned with a scintillation detector and K_β filter with the x-ray generator set at 40 kV and 80 mA and the cementite peaks scanned with a solid state detector at 40 kV and 160 mA. The scans were all done automatically under PC based computer control[15] and the data stored for later analysis. The matrix scans were done at 0.1° intervals from 153.5 to 159° 2θ for 2 seconds a point. The cementite scans were done in three regions. The tails were scanned in 0.1° intervals from 145 to 147° and from 149 to 151° for 10 seconds and the peak region scanned at 0.05° intervals from 147 to 149° for 20 to 40 seconds a point. For higher sample tilts the peak region was scanned for the longer time intervals to compensate for peak broadening due to defocusing of the x-ray optics from tilting the sample.

Peaks were obtained at ψ = 0, 18.43, 26.57, 33.21, 39.23, and 45° for ϕ values of 0, 60, 120, 180, 240, and 300°. The ψ tilts were achieved with ω-goniometry, tilting in the diffraction plane.[7] After collecting the data and determining the peak positions the deviatoric stresses were determined by least squares fitting the data to Equation 10. For a single specimen the data could be collected and analyzed in about 20 hours.

C. *Diffraction Elastic Constants*

The diffraction elastic constants for both the matrix and cementite phases were measured for all three microstructures by standard techniques.[7,10] A tensile device[10] was put on the diffractometer and a biaxial stress measurement along the loading direction performed at a number of applied loads with the same experimental parameters previously described.

D. *Fatigue Loading*

Loading was carried out on an MTS 100 kN servo-hydraulic fatigue machine at room temperature. The specimens were loaded in total strain control with a

triangular waveform and a strain amplitude of $\Delta\varepsilon/2=0.005$. The strain rate was 3.3×10^{-3} s^{-1} for the pearlitic and spheroidized samples and 2.5×10^{-4} s^{-1} for the tempered martensite. The tempered martensite specimens were loaded at a slower rate because, at their strength levels, the capacity of the fatigue machine was approached. Load-extension hysteresis loops were recorded from the load cell and extensometer from which the applied deviatoric macro-stress tensor can be written as:

$$ {}^{Appl}\tau_{ij} = \begin{bmatrix} 2P/3A & 0 & 0 \\ 0 & -P/3A & 0 \\ 0 & 0 & -P/3A \end{bmatrix} $$

where P is the applied force and A is the specimen cross sectional area.

A specimens was loaded and a test stopped at different points around the stress-strain hysteresis loop. The hydraulics were turned off and the sample allowed to relax elastically to zero applied stress. It was then removed and the residual stresses measured.

IV. Results

The diffraction elastic constants are presented in Table I. Note that the ferrite and cementite have similar elastic properties. This means that any micro-stresses due to elastic incompatibility of the two phases will be small. This will help us to reconstruct the stress response of the individual phases because the micro-stresses will be due only to differential plastic behavior. Cementite has a tetragonal crystal structure[16] and its elastic properties will be anisotropic.[17] However, these effects will be small compared to the micro-stresses arising from plastic deformation.

The pearlitic steel showed an initial distinct yield point and then quickly formed a stable hysteresis loop, shown in Figure 5. Four companion specimens were run and stopped at each quarter cycle on the eleventh fatigue cycle. The spheroidite behaved similar to the pearlite, showing an initial yield point and then quickly forming a stable hysteresis loop as shown in Figure 6. Four companion specimens were also stopped at each quarter cycle on the eleventh fatigue cycle for the spheroidite. Figure 7 shows the first and fifth fatigue cycles for the tempered martensite. The much stronger

microstructure only yields a small amount at 0.005 strain and cyclically softened. Two specimens were measured on the first cycle at the 1/4 and 3/4 cycle positions, and two specimens were examined on the fifth cycle at the same 1/4 and 3/4 cycle positions to attempt to observe the effects of the cyclic softening.

Figure 5 also shows the individual stress responses for the ferrite and cementite phases in pearlite. As indicated above, only four points were measured but the general form of the curves may be determined. After reversal of the applied strain at the maximum and minimum strain values the matrix and cementite will relax elastically until the bulk material begins to yield. The response in both phases may be assumed to be elastic with a slope equal to the bulk because the measured diffraction elastic constants are the same for the two phases. The micro-stresses are constant in this region because they arise from the plastic incompatibility of the two phases and the material is behaving elastically in this region. After the bulk material yields the curves for the two phases are assumed to vary smoothly and pass through the measured points. The micro-stresses are changing because the two phases have a different plastic response to the applied strain.

Table II gives the measured residual macro-stress and micro-stress tensors and Table III gives the applied stress tensors computed from the load cell on the fatigue machine. The results for the individual phases in the spheroidite are given in Figure 6. Curves for the individual phases in the tempered martensite are not shown in Figure 7 because only the end points were measured and the situation appears to be more complicated. From Table II we see that after unloading a significant macro-stress exists. The tensile and compressive macro-stresses upon unloading from compression and tension respectively, indicate that the surface of the specimens yielded before the interiors. The same is true to a smaller extent for the pearlitic specimens.

V. Discussion

Via diffraction, we have shown here that it is possible to separate the average stress response of a two-phase material into components for the individual phases. Such measurements give us a more complete understanding of the material's behavior. In 1080 steel we see that the component phases behave very differently and interact to produce the bulk mechanical behavior of the material. From the hysteresis loops we see that the micro-stresses changes continuously during loading. As the matrix

alternately yields in tension and compression the proportion of the stress on the bulk material taken by the cementite increases. Thus the stress range in the cementite is greater and the stress range in the ferrite is smaller than the stress range experienced by the bulk material.

Low cycle fatigue tests are used to represent the behavior of the material at a stress concentration or at the tip of a fatigue crack where cyclic strains control the materials response to fatigue loading.[18] Theories for fatigue crack growth do not as yet take into account the nonuniform plastic field at a crack tip advancing through a two-phase material and the higher stress range experienced by the harder phase shown by this study. Fatigue cracks that have a size comparable to the microstructure are known to grow anomalously fast[19,20] and may be affected by these alternating micro-stresses in the microstructure. Large cracks will see an average of a large portion of the microstructure at the crack front.

This work also has implications for diffraction measurements of residual stresses used for quality control or in service measurements of parts. These measurements of residual stresses are attractive because they are nondestructive. The ability to measure both macro- and micro-stresses further enhances these methods attractiveness. Traditional measurements on steel only measure the stresses in the ferrite phase. A compressive stress measured in the matrix phase has been viewed as beneficial to the fatigue resistance. This is true if the stress is a macro-stress. If the compressive stress measured in the ferrite is a micro-stress it will mean that a much larger tensile stress exists in the cementite and this will not provide the desired fatigue resistance. Which state exists may not be determined without measuring the stresses in the carbides. In multiphase materials it is important to measure the stresses present in all the phases. Previous measurements of residual stresses and their changes with fatigue in multiphase materials need to be reexamined.

VI. Conclusions

(1) We have demonstrated that diffraction is an important and useful tool for studying the individual responses of phases in multiphase or composite materials to mechanical loading. In particular, the stress strain hysteresis loop for 1080 steels with different microstructures has been separated into components for the matrix and cementite phases.

(2) As steel deforms in fatigue, the fraction of the load taken by the carbides greatly increases. In low cycle strain controlled fatigue the stress range $\Delta\sigma$ is much higher in the carbides than for the bulk material.

(3) The fatigue deformation of a two phase material will leave residual micro-stresses in each phase which depend on the final deformation state and on the path to that state. Residual macro-stresses are also possible. Stress measurements in only one phase of a two phase material may be inadequate to understand mechanical properties unless the stress in the other phase can be inferred with some confidence, for example from previous measurements in that phase.

(4) The diffraction elastic constants in ferrite and cementite were measured and found to be similar in pearlite, spheroidite, and tempered martensite in 1080 steel.

Acknowledgments

This research was supported by the Office of Naval Research under contract No. N00014-80-C-116. This work made use of the Northwestern X-ray Diffraction Facility supported in part by the National Science Foundation through the Northwestern University Materials Research Center, Grant No. DMR 8821571. This research represents a portion of a thesis submitted (by R.A.W.) to Northwestern University in partial fulfillment of the requirements fot the Ph.D. degree.

References

[1] D.V. Wilson and Y.A. Konnan: *Acta Met.*, 1964, vol. 12, pp. 617-628.

[2] Takao Hanabusa, Jiro Fukura, and Haruo Fujiwara: *Bull. J.S.M.E.*, 1969, vol. 12, pp. 931-939.

[3] D.J. Quesnel, M. Meshii, and J.B. Cohen: *Mat. Sci. Engr.*, 1978, vol. **36**, pp. 207-215.

[4] D.J. Quesnel and M. Meshii: *Mat. Sci. Engr.*, 1977, vol. 30, pp. 223-241.

[5] I.C. Noyan: *Met. Trans.* A, 1983, vol. 14A, pp. 1907-1914.

[6] J.B. Cohen: *Powder Diffraction*, 1986, vol. **1**, pp. 15-21.

[7] I.C. Noyan and J.B. Cohen: *Residual Stress: Measurement by Diffraction and Interpretation*, Springer-Verlag, New York, 1987.

[8] H. Dölle: *J. Appl. Cryst.*, 1979, vol. 12, pp. 489-501.

[9] R.A. Winholtz and J.B. Cohen: *Aust. J. Phys.*, 1988, vol. 41, pp. 189-199.

[10] K. Perry, I.C. Noyan, P.J. Rudnick, and J.B. Cohen: *Adv. X-ray Anal.*, 1984, vol. 27, pp. 159-170.

[11] I.C. Noyan: *Adv. X-ray Anal.*, 1985, vol. 28, pp. 178-185.

[12] R.A. Winholtz and J.B. Cohen: *Adv. X-ray Analysis*, 1989, vol. **32**, pp. 341-353.

[13] G.K. Wertheim, M.A. Butler, K.W. West, and D.N.E. Buchanan: *Rev. Sci. Instrum.*, 1974, vol. **45**, pp. 1369-1371.

[14] William H. Press, Brian P. Flannery, Saul Teukolsky, and William T. Vetterling: *Numerical Recipes: The Art of Scientific Computing*, Cambridge University Press, Cambridge, 1986. pp. 521-528.

[15] R.A. Winholtz: ONR Technical Report #27, 1990.

[16] E.J. Fasiska and G.A. Jeffrey: *Acta Cryst.*, 1965, vol. 19, pp. 463-471.

[17] A. Kagawa, T. Okamoto, and H. Matsumoto: *Acta Met.*, 1987, vol. 35, pp. 797-803.

[18] *Manual on Low Cycle Fatigue Testing*, ASTM *STP465*, 1969.

[19] S. Suresh and R.O. Ritchie: *Int. Rev. Metals*, 1984, vol. 29, pp. 445-476.

[20] R.O. Ritchie and J. Lankford, Eds.: *Small Fatigue Cracks*, TMS-AIME, Warrendale, PA, 1986.

Table I

Diffraction Elastic Constants for 1080 Steel (x 10^{-6} MPa^{-1})*

		S_1	$S_2/2$
Pearlite	Ferrite	-1.29 ± 0.02	5.11 ± 0.06
	Cementite	-1.38 ± 0.07	4.88 ± 0.22
Spheroidite	Ferrite	-1.26 ± 0.02	4.97 ± 0.06
	Cementite	-1.29 ± 0.07	4.91 ± 0.22
Tempered Martensite	Ferrite	-1.27 ± 0.03	5.58 ± 0.08
	Cementite	-2.11 ± 0.12	5.47 ± 0.30

* For the 211 ferrite peak and the 250 cementite peak

Table II

Measured Deviatoric Macro- and Micro-Stress Tensors in Fatigued 1080 Steel

(a) Macro-Stresses (MPa)

Sample	Micro-structure	Cycles	$^{M}\tau_{11}$	$^{M}\tau_{22}$	$^{M}\tau_{33}$	$^{M}\tau_{12}$	$^{M}\tau_{13}$	$^{M}\tau_{23}$
A8	P	10.00	9.87 (2.57)	-6.49 (2.57)	-1.38 (1.97)	-2.39 (1.55)	-1.83 (0.26)	-0.21 (0.21)
A14	P	10.25	-54.59 (13.20)	27.55 (8.74)	27.03 (7.06)	-5.07 (1.54)	-1.70 (0.59)	-0.85 (0.52)
A9	P	10.50	-5.56 (2.90)	7.55 (2.59)	-1.99 (2.34)	-0.51 (0.65)	-0.08 (0.22)	0.73 (0.22)
A17	P	10.75	22.95 (9.91)	0.32 (7. 60)	-23.27 (4.32)	-1.47 (0.98)	0.05 (0.35)	0.50 (0.40)
A21	S	10.00	0.39 (3.25)	1.45 (2 .73)	-1.85 (1.70)	-2.15 (0.70)	-0.68 (0.27)	-0.94 (0.24)
A23	S	10.25	-16.53 (7.96)	9.50 (3. 21)	7.03 (6.22)	5.63 (2.85)	0.48 (0.30)	2.21 (0.76)
A22	S	10.50	-4.88 (2.93)	1.01 (2 .41)	3.86 (1.88)	-0.81 (0.79)	0.15 (0.24)	-0.27 (0.34)
A24	S	10.75	3.67 (7.75)	4.61 (5 .27)	-8.28 (3.42)	-0.75 (0.78)	-1.24 (0.39)	-1.25 (0.29)
A37	TM	0.25	-92.93 (11.60)	9.26 (10.90)	83.68 (12.40)	-3.48 (2.63)	-2.16 (1.00)	2.54 (1.23)
A39	TM	0.75	88.82 (14.33)	-12.31 (12.63)	-76.51 (13.35)	-1.50 (2.30)	0.13 (0.94)	-1.27 (0.83)
A38	TM	4.25	-69.71 (14.74)	4.81 (15.02)	64.90 (16.15)	-1.69 (3.31)	-1.23 (1.24)	-2.39 (1.34)
A43	TM	4.75	82.52 (19.24)	-1.34 (16.78)	-81.18 (15.40)	0.66 (2.45)	-2.34 (1.10)	-0.59 (1.00)

(b) Micro-Stresses Ferrite (MPa)

Sample	Micro-structure	Cycles	$^{\mu,\alpha}\tau_{11}$	$^{\mu,\alpha}\tau_{22}$	$^{\mu,\alpha}\tau_{33}$	$^{\mu,\alpha}\tau_{12}$	$^{\mu,\alpha}\tau_{13}$	$^{\mu,\alpha}\tau_{23}$
A8	P	10.00	1.60 (2.26)	-2.34 (2.33)	-1.25 (1.78)	3.63 (1.57)	0.13 (0.16)	0.07 (0.15)
A14	P	10.25	-37.35 (16.44)	20.33 (10.03)	17.02 (8.31)	1.69 (1.28)	0.77 (0.51)	0.46 (0.46)
A9	P	10.50	-4.17 (2.80)	1.07 (2.23)	3.09 (2.18)	0.79 (0 53)	0.21 (0.18)	-0.01 (0.16)
A17	P	10.75	26.74 (11.74)	-17.15 (8.02)	-9.58 (4.96)	-0.97 (0.82)	0.22 (0.29)	-0.52 (0.34)
A21	S	10.00	6.55 (3.00)	-4.27 (2.16)	-2.27 (1.30)	-1.04 (0.54)	0.33 (0.18)	-0.33 (0.18)
A23	S	10.25	-21.83 (9.33)	5.15 (2.92)	16.68 (7.11)	-6.73 (2.85)	-0.16 (0.22)	-1.62 (0.71)
A22	S	10.50	-5.35 (2.74)	2.32 (1.80)	3.03 (1.69)	1.18 (0.63)	-0.15 (0.16)	-0.72 (0.33)
A24	S	10.75	19.90 (8.52)	-11.51 (5.15)	-8.39 (3.75)	0.26 (0.50)	0.56 (0.30)	-0.16 (0.19)
A37	TM	0.25	-20.01 (12.75)	14.43 (11.32)	5.58 (11.57)	-3.56 (2.73)	1.01 (0.95)	-1.83 (1.19)
A39	TM	0.75	33.76 (17.31)	-18.45 (13.25)	-15 .31 (13.92)	-2.30 (2.28)	0.10 (0.92)	-0.17 (0.80)
A38	TM	4.25	-23.58 (16.10)	16.77 (15.24)	6.81 (15.91)	2.92 (3.21)	0.58 (1.19)	1.03 (1.27)
A43	TM	4.75	49.21 (23.45)	-29.73 (17.65)	-19 .48 (16.33)	1.01 (2.36)	0.59 (1.04)	-0.95 (0.99)

(c) Micro-Stresses Cementite (MPa)

Sample	Micro-structure	Cycles	$^{\mu,\beta}\tau_{11}$	$^{\mu,\beta}\tau_{22}$	$^{\mu,\beta}\tau_{33}$	$^{\mu,\beta}\tau_{12}$	$^{\mu,\beta}\tau_{13}$	$^{\mu,\beta}\tau_{23}$
A8	P	10.00	-11.71 (15.84)	17.17 (15.55)	9.14 (12.53)	-26.61 (3.36)	-0.98 (1.12)	-0.48 (1.09)
A14	P	10.25	273.88 (41.96)	-149.08 (40.34)	-124.80 (32.59)	-12.42 (7.87)	-5.66 (2.89)	-3.36 (3.06)
A9	P	10.50	30.57 (16.24)	-7.87 (16. 04)	-22.69 (13.00)	-5.78 (3.10)	-1.51 (1.16)	0.05 (1.15)
A17	P	10.75	-196.06 (29.29)	125.78 (27.67)	70.29 (21.92)	7.11 (5.21)	-1.60 (2.00)	3.81 (1.95)
A21	S	10.00	-48.02 (9.57)	31.34 (9. 17)	16.68 (6.59)	7.62 (2.45)	-2.42 (0.88)	2.40 (0.88)
A23	S	10.25	160.08 (17.88)	-37.75 (14.72)	-122.33 (12.92)	49.32 (4.67)	1.15 (1.52)	11.88 (1.68)
A22	S	10.50	39.21 (11.86)	-17.01 (11.19)	-22.20 (8.30)	-8.65 (2.96)	1.10 (1.09)	5.28 (1.10)
A24	S	10.75	-145.94 (16.49)	84.44 (14.52)	61.50 (10.67)	-1.93 (3.57)	-4.10 (1.35)	1.20 (1.31)
A37	TM	0.25	146.75 (71.27)	-105.82 (70.56)	-40.94 (83.12)	26.12 (16.84)	-7.39 (6.25)	13.42 (6.71)
A39	TM	0.75	-247.57 (75.31)	135.27 (79.53)	112.30 (90.92)	16.88 (15.22)	-0.72 (6.71)	1.25 (5.82)
A38	TM	4.25	172.91 (94.05)	-122.96 (99.53)	-49.95 (114.82)	-21.40 (21.82)	-4.25 (8.57)	-7.53 (8.76)
A43	TM	4.75	-360.85 (85.99)	218.04 (92.99)	142.82 (104.26)	-7.40 (17.06)	-4.35 (7.41)	6.94 (6.66)

Table III

Applied Stresses (MPa)

Sample	Micro-structure	Cycles	$^{Appl}\tau_{11}$	$^{Appl}\tau_{22}$	$^{Appl}\tau_{33}$	$^{Appl}\tau_{12}$	$^{Appl}\tau_{13}$	$^{Appl}\tau_{23}$
A8	P	10.00	200.17	-100.08	-100.08	0.00	0.00	0.00
A14	P	10.25	311.14	-155.57	-155.57	0.00	0.00	0.00
A9	P	10.50	-200.04	100.02	100.02	0.00	0.00	0.00
A17	P	10.75	-311.14	155.57	155.57	0.00	0.00	0.00
A21	S	10.00	179.09	-89.55	-89.55	0.00	0.00	0.00
A23	S	10.25	272.75	-136.38	-136.38	0.00	0.00	0.00
A22	S	10.50	-173.12	86.56	86.56	0.00	0.00	0.00
A24	S	10.75	-270.67	135.33	135.33	0.00	0.00	0.00
A37	TM	0.25	713.52	-356.76	-356.76	0.00	0.00	0.00
A39	TM	0.75	-750.06	375.03	375.03	0.00	0.00	0.00
A38	TM	4.25	633.17	-316.59	-316.59	0.00	0.00	0.00
A43	TM	4.75	-703.88	351.94	351.94	0.00	0.00	0.00

Figure 1. Coordinate systems used in stress measurements with diffraction.

Figure 2. Mechanical behavior of a two-phase material.

Figure 3. Dimensions of fatigue specimens used. All dimensions in mm.

Figure 4. 250 diffraction peak for cementite.

Figure 5. Hysteresis loop for pearlitc 1080 steel with component for the matrix and cementite phases.

Figure 6. Hysteresis loop for spheroiditic 1080 steel with component for the matrix and cementite phases.

Figure 7. Hysteresis loops for tempered martensitic 1080 steel. (a) The first fatigue cycle along with the stresses in the matrix and cementite. (b) The fifth fatigue cycle along with the stresses in the matrix and cementite.

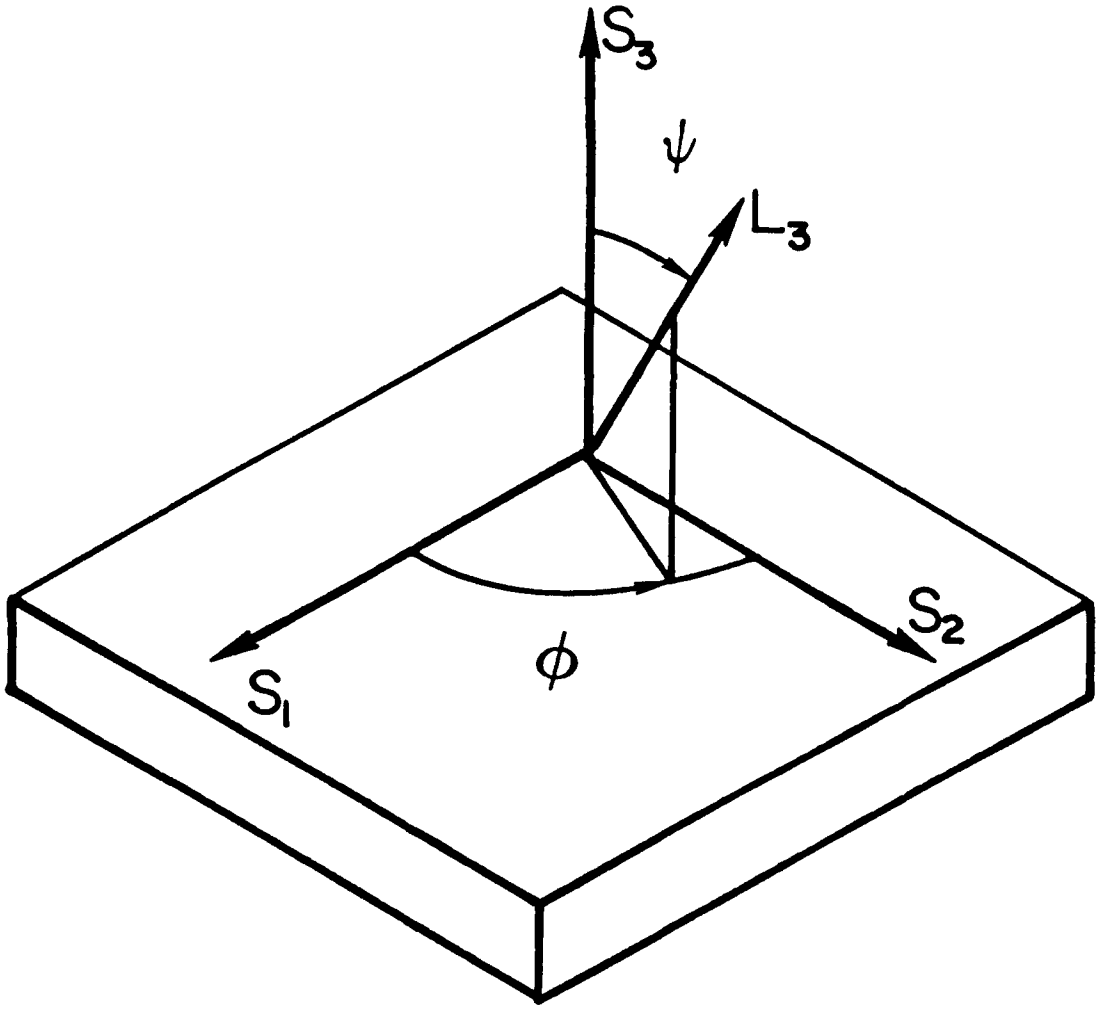

Figure 1. Coordinate systems used in stress measurements with diffraction.

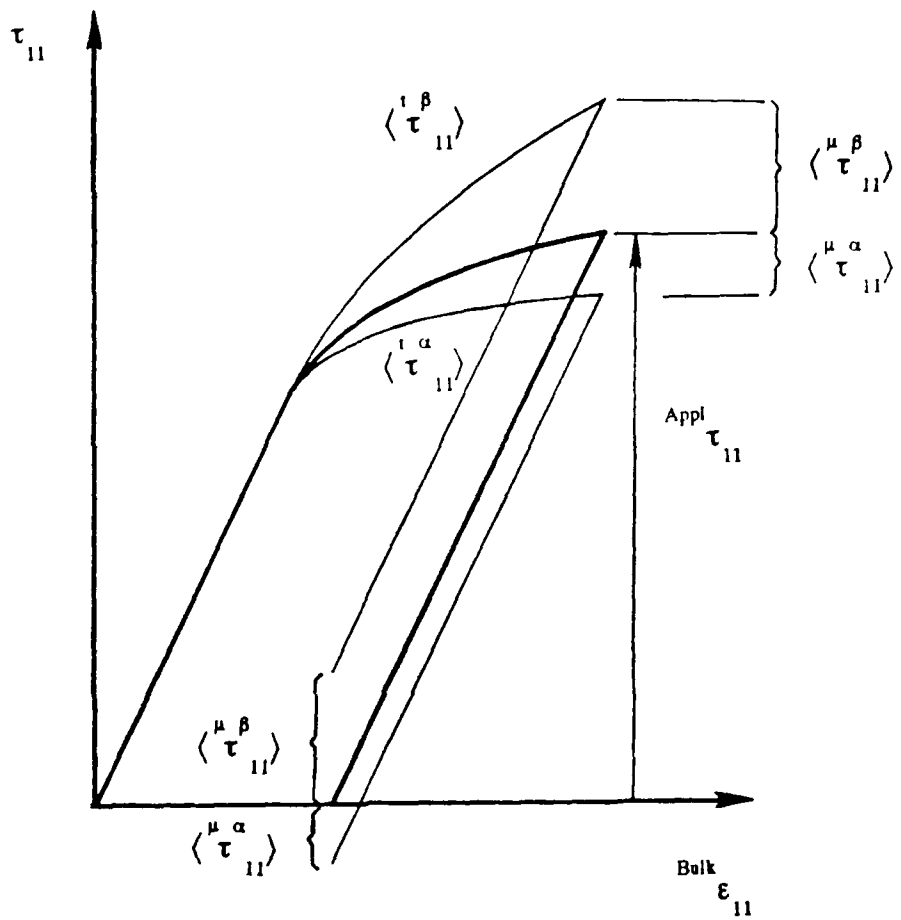

Figure 2. Mechanical behavior of a two-phase material.

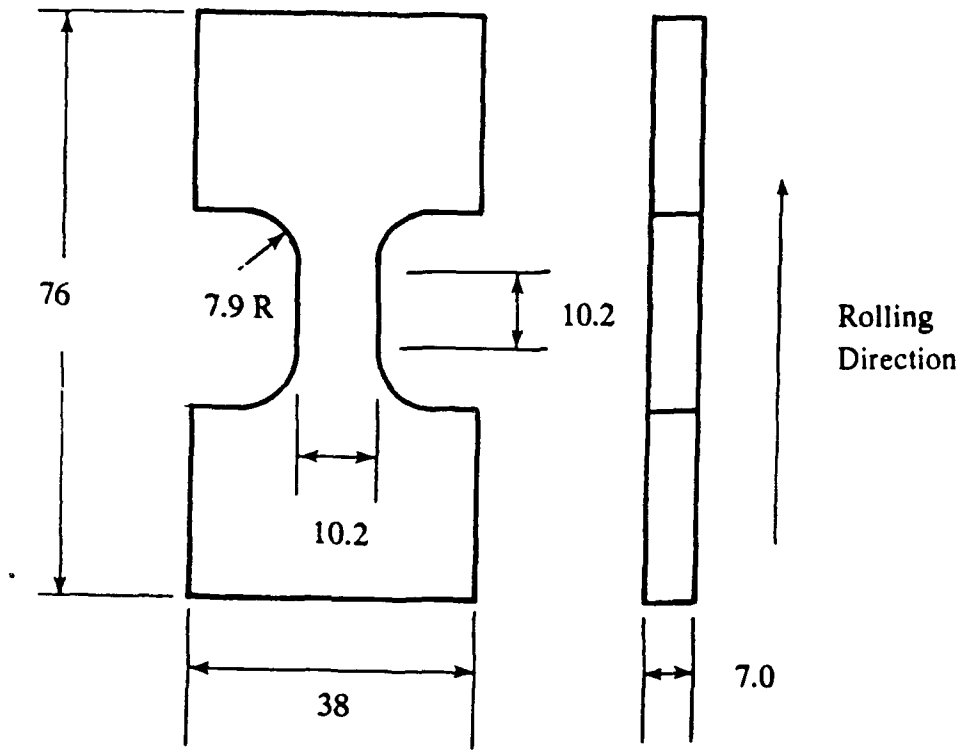

Figure 3. Dimensions of fatigue specimens used. All dimensions in mm.

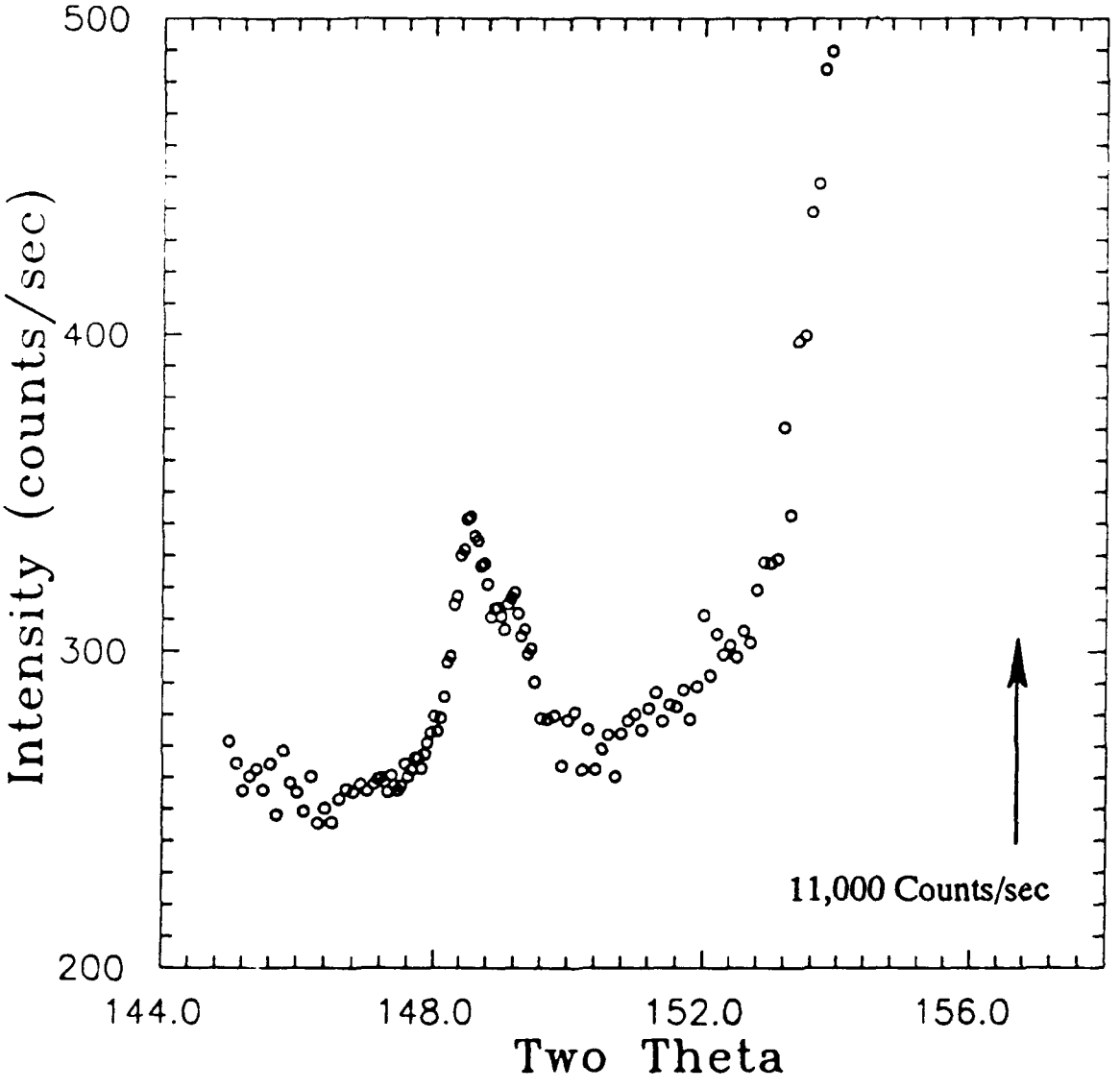

Figure 4. 250 diffraction peak for cementite.

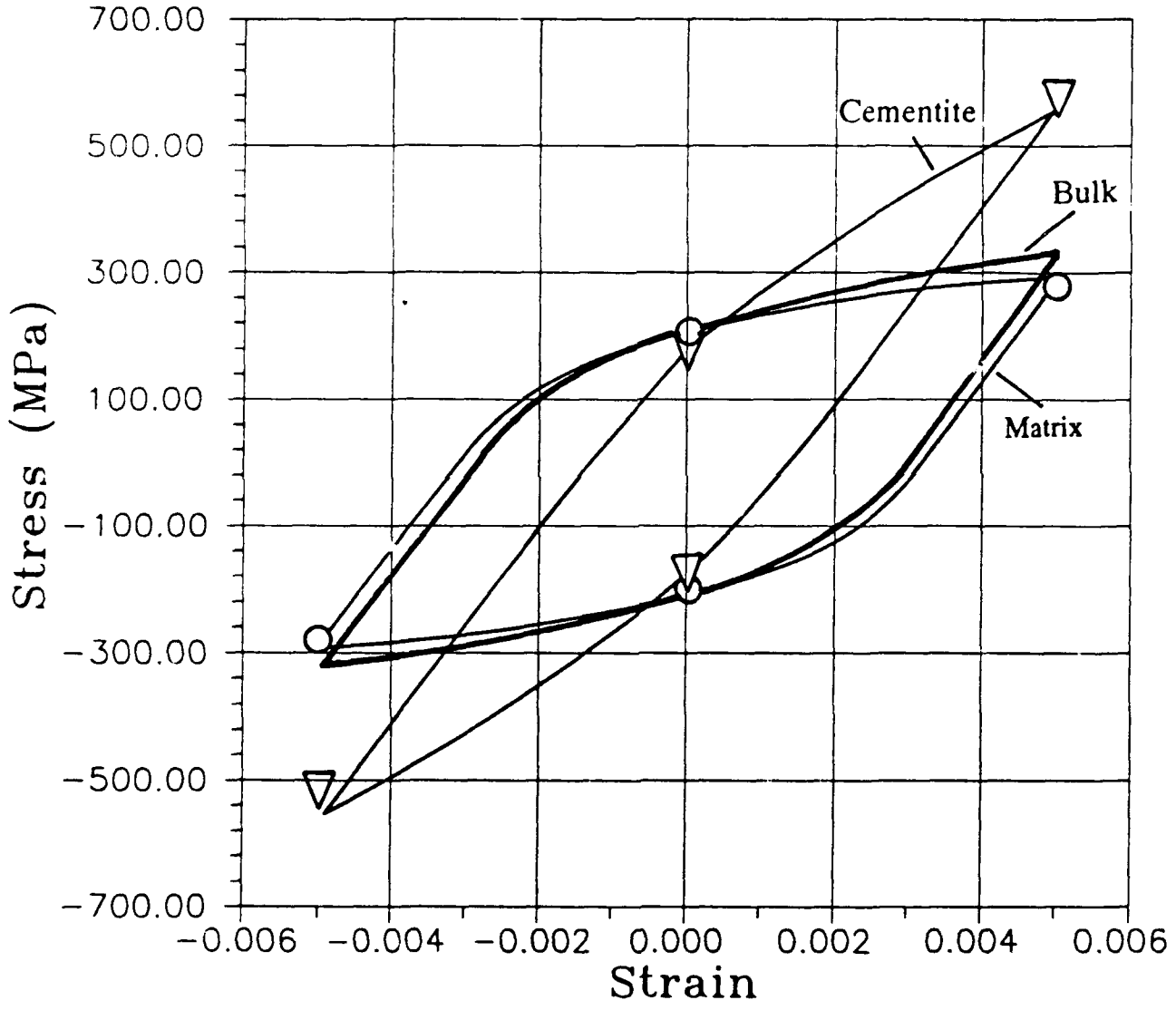

Figure 5. Hysteresis loop for pearlitc 1080 steel with component for the matrix and cementite phases.

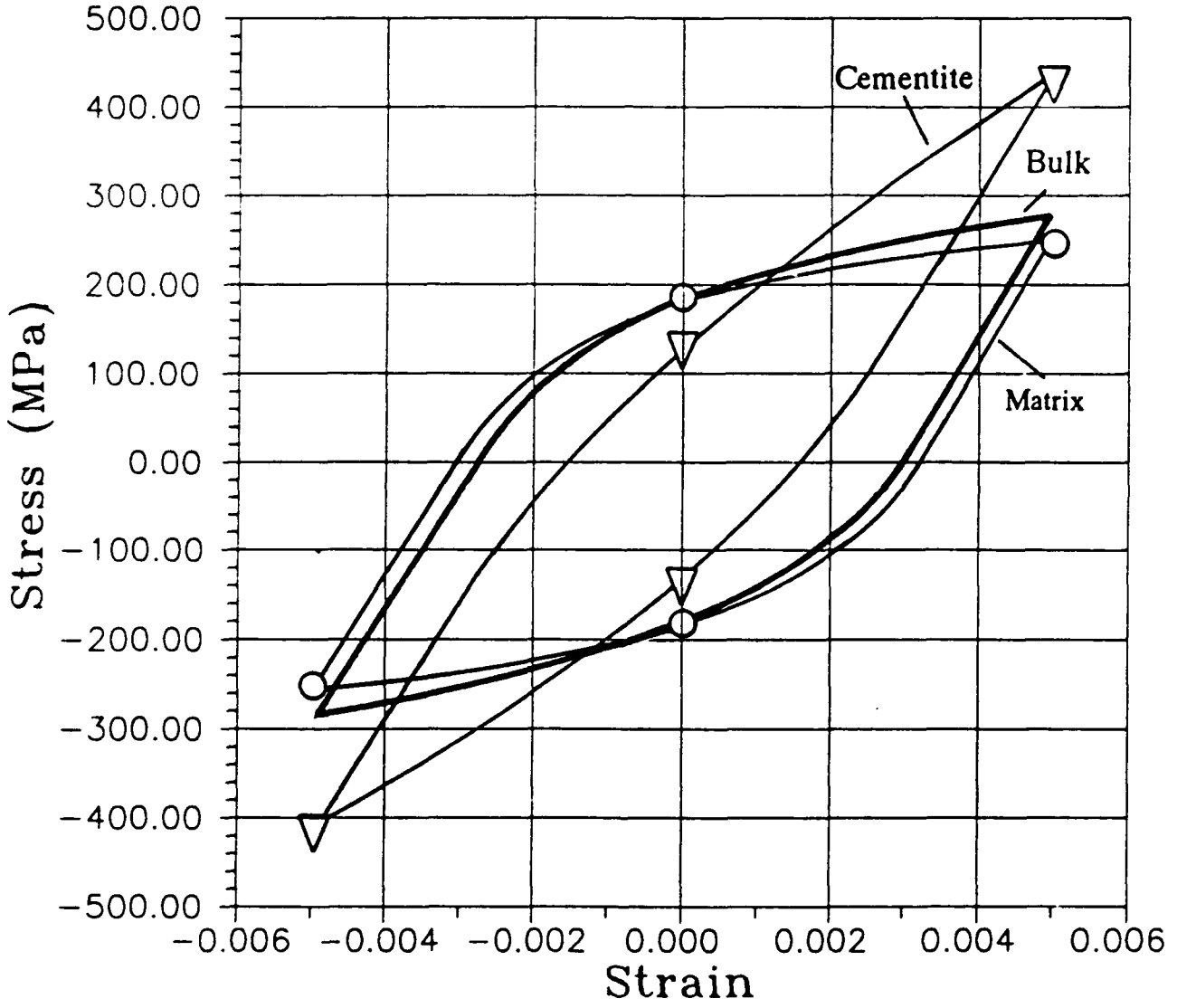

Figure 6. Hysteresis loop for spheroiditic 1080 steel with component for the matrix and cementite phases.

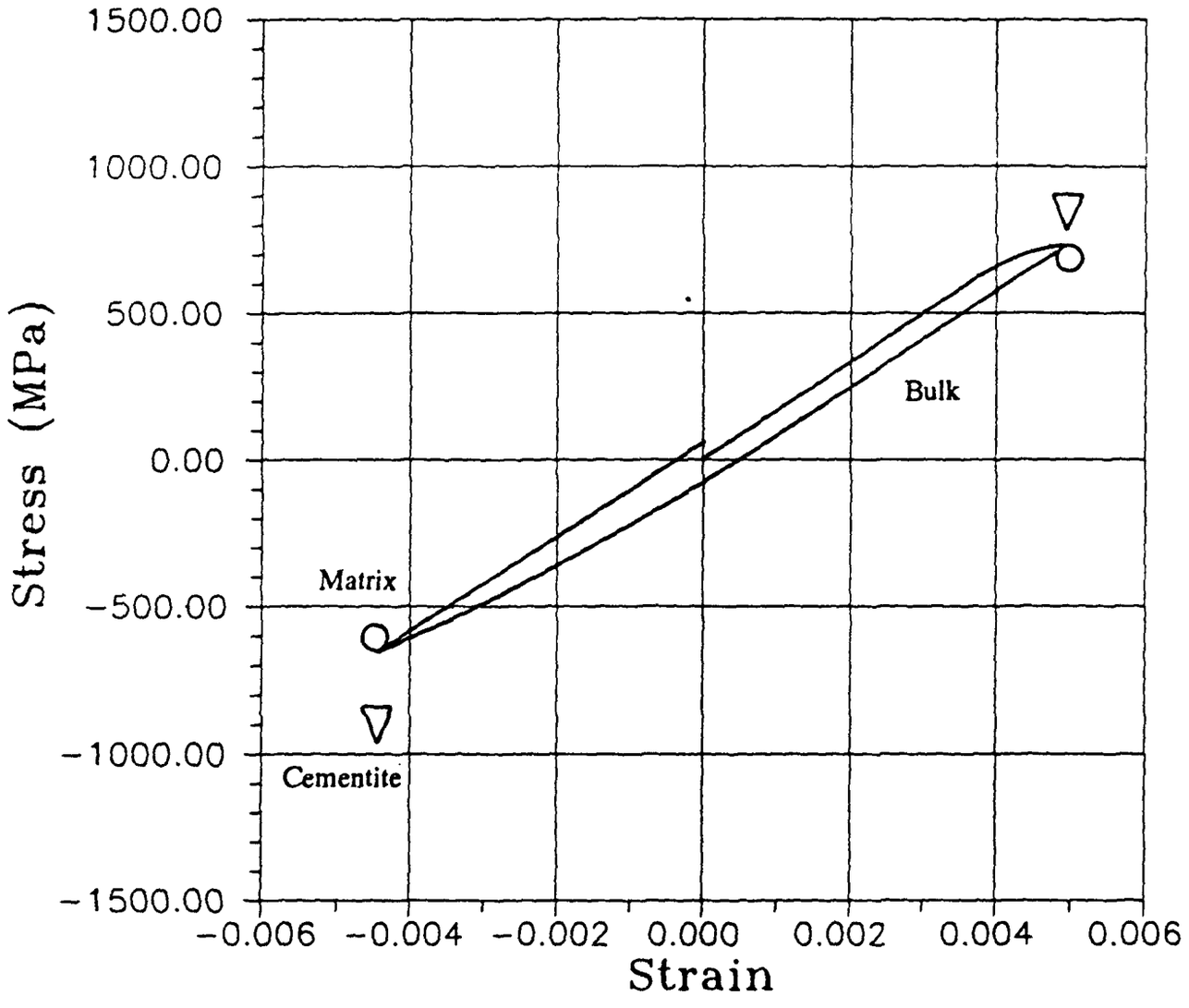

(a)

Figure 7. Hysteresis loops for tempered martensitic 1080 steel. (a) The first fatigue cycle along with the stresses in the matrix and cementite. (b) The fifth fatigue cycle along with the stresses in the matrix and cementite.

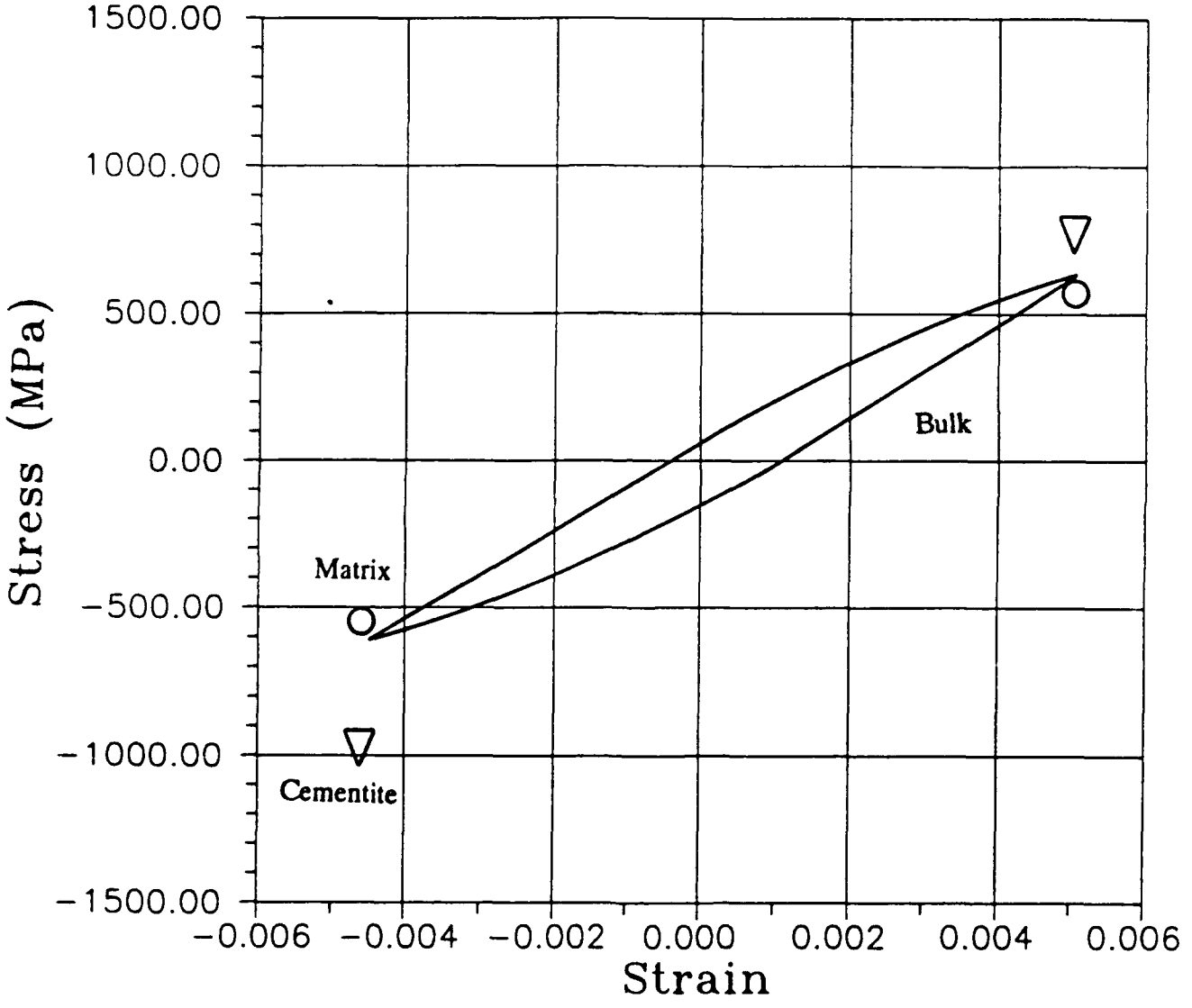
1500.00
1000.00
500.00
0.00
-500.00
-1000.00
-1500.00
Stress (MPa)
-0.006
-0.004
-0.002
0.000
0.002
0.004
0.006
Strain
Bulk
Matrix
Cementite

(b)

Security Classification

DOCUMENT CONTROL DATA - R & D

(Security classification of title, body of abstract and indexing annotation must be entered when the overall report is classified)

1. ORIGINATING ACTIVITY *(Corporate author)*

J. B. Cohen
McCormick School of Engineering & Applied Science
Northwestern University, Evanston, IL 60208

2a. REPORT SECURITY CLASSIFICATION

2b. GROUP

3. REPORT TITLE

LOAD SHARING OF THE PHASES IN 1080 STEEL DURING LOW CYCLE FATIGUE

4. DESCRIPTIVE NOTES *(Type of report and inclusive dates)*

TECHNICAL REPORT # 28

5. AUTHOR(S) *(First name, middle initial, last name)*

R. A. WINHOLTZ AND J. B. COHEN

6. REPORT DATE

NOVEMBER 1990

7a. TOTAL NO. OF PAGES

30 pages

7b. NO. OF REFS

8a. CONTRACT OR GRANT NO.

N00014-80-C-116

b. PROJECT NO.

c.

d.

9a. ORIGINATOR'S REPORT NUMBER(S)

28

9b. OTHER REPORT NO(S) *(Any other numbers that may be assigned this report)*

10. DISTRIBUTION STATEMENT

Distribution of document is unlimited

11. SUPPLEMENTARY NOTES

12. SPONSORING MILITARY ACTIVITY

Metallurgy Branch
Office of Naval Research

13. ABSTRACT

By means of x-ray diffraction, the stress response of the individual phases in a 1080 steel were measured. Specimens with pearlitic, spheroidal, and tempered martensitic microstructures were subjected to low cycle fatigue and the stress strain hysteresis loops were separated into components for the carbide and matrix phases. These results show that as the material yields in both tension and compression the carbides take a higher fraction of the load and thus the stress range experienced by the carbide phase is much higher than the matrix during low cycle fatigue.

DD FORM 1 NOV 1473 (PAGE 1)

S/N 0101-807-6801

Security Classification

14 KEY WORDS	LINK A		LINK B		LINK C	
	ROLE	WT	ROLE	WT	ROLE	WT